

# Heterogeneous Force Chains in Cellularized Biopolymer Networks

Long Liang<sup>1</sup>, Christopher Jones<sup>2</sup>, Bo Sun<sup>2</sup>, and Yang Jiao<sup>1,3,\*</sup>

<sup>1</sup>*Department of Physics, Arizona State University, Tempe, AZ, 85287*

<sup>2</sup>*Department of Physics, Oregon State University, Corvallis, OR, 97331 and*

<sup>3</sup>*Materials Science and Engineering, Arizona State University, Tempe, AZ 85287\**

Biopolymer Networks play an important role in coordinating and regulating collective cellular dynamics via a number of signaling pathways. Here, we investigate the mechanical response of a model biopolymer network due to the active contraction of embedded cells. Specifically, a graph (bond-node) model derived from confocal microscopy data is used to represent the network microstructure, and cell contraction is modeled by applying correlated displacements at specific nodes, representing the focal adhesion sites. A force-based stochastic relaxation method is employed to obtain force-balanced network under cell contraction. We find that the majority of the forces are carried by a small number of heterogeneous force chains emitted from the contracting cells. The force chains consist of fiber segments that either possess a high degree of alignment before cell contraction or are aligned due to the reorientation induced by cell contraction. Large fluctuations of the forces along different force chains are observed. Importantly, the decay of the forces along the force chains is significantly slower than the decay of radially averaged forces in the system. These results suggest that the fibrous nature of biopolymer network structure can support long-range force transmission and thus, long-range mechanical signaling between cells.

PACS numbers: 87.15.rp, 87.85.jc

## 1. INTRODUCTION

The extracellular matrix (ECM) is an interconnected network of biopolymers that provides structural support for cells and allows the diffusion of biochemicals within tissues. The most abundant component of ECM is type I collagen, a fibrous protein responsible for giving the ECM its material stiffness [1]. Cells attach and move through the ECM using protein complexes that link the ECM to the force-generating cell cytoskeleton [2]. However, these cell-ECM adhesions also act as sensors, sending information to the cell about the structure and mechanical properties of the surrounding matrix [3, 4] and helping to regulate cell behavior such as motility, morphology, and differentiation [5–7]. The stiffness and the relative alignment of fibers in the network are particularly important to cell function. For example, dense and rigid collagen gel can promote growth and progression of cancer cells and tumors [8, 9]. Other important examples are durotaxis in which cells tend to move in the direction of increasing matrix stiffness [10], and contact guidance in which cells tend to align and move in the direction of fiber alignment [11, 12].

Cell-ECM interaction is a dynamic process in which the cell actively remodels the network [4, 13] and these effects can propagate over long distances, even affecting the bulk properties of the network [14, 15]. Specifically, tension exerted by the cells can align the fibers in the network leading to long range force transmission [14, 16, 17]. Fiber mediated stresses can trigger mechano-sensitive pathways of distant cells affecting behaviors such as force

generation [18, 19] and cell-ECM adhesions [20] and leading to diverse collective behaviors [21]. This coupling of cells provides a means for mechanical communication and plays an important role in regulating and coordinating collective cellular dynamics in a wide range of biophysical processes, such as morphogenesis, tissue regeneration, and immune response, as well as diseases such as muscular dystrophy, fibrosis, and cancer [4, 13, 22–25].

Due to their effect on cell behavior and communication, a significant amount of work has been carried out to characterize the structural and physical properties of biopolymer networks. Traditional morphological descriptors for such networks include the distribution of fiber length [26], porosity [27, 28], pore-size distribution [29–32] and turbidity [33, 34], which are mainly bulk averaged properties. Recently, local topological and geometrical statistics such as distribution of number of fibers at a cross-link node (i.e., valency number) and relative fiber orientations (i.e., direction cosine) are employed to successfully reconstruct type I collagen (COL-I) network computationally [35]. Higher order spatial fluctuations have also been utilized to characterize the evolution of COL-I network during gelation process [36]. In addition, the transport properties (e.g., macromolecule diffusivity) [32, 37–46] and mechanical properties (e.g., elastic moduli, bulk rheology, stress distribution, etc.) [14, 16, 18, 35, 47–53] of biopolymer network, which are respectively crucial to the chemical and mechanical signaling between the cells, strongly depend on the network microstructure.

In most studies, the biopolymer network is treated as a material system with no biological cells embedded. However, it is known that cellular interaction with COL-I can induce dynamic remodeling of the network. These cellular scale dynamics propagate to much longer range and affect the bulk properties of the network [15], as well

---

\*Electronic address: yang.jiao.2@asu.edu

as the behavior of other cells through mechano-sensitive pathways and machineries [13, 24, 25]. In addition, fiber mediated stress-regulated force generation [18, 19] and stress-reinforced cell-ECM adhesion [20] provide internal feedback mechanisms that support the emergence of diverse collective behaviors [21]. As a result, understanding the homeostasis of cellularized biopolymer network is an essential step towards the understanding of complex, self-organized multicellular dynamics [23].

Recently, continuum models of cellularized collagen network have been developed to investigate the fiber-mediated mechanical coupling between the cells [16, 54]. Specifically, high-resolution 2D confocal images of cellularized ECM are thresholded to generate a three-phase heterogeneous system including a cell phase, a fiber phase and an interstitial fluid phase [16]. Finite element analysis is then employed to obtain stress distribution in the ECM. It has been shown that explicitly considering the fibrous nature of ECM is necessary to capture the force transmission between cell pairs [16] and the invasion of cancer cells in ECM with well defined geometry [54]. Such behaviors can not be correctly reproduced using either linear or nonlinear homogeneous ECM models. Despite all these insights, the continuum models do not explicitly incorporate cell induced fiber re-orientation and other structural remodeling mechanisms for cellularized ECM, and thus might not accurately reveal the pathways for force transmission in the system [14].

In this paper, we systematically investigated the mechanical behavior of cellularized ECM, in particular, fiber-mediated transmission of forces generated by active contraction of embedded cells. The biopolymer network is represented by a graph (i.e., bond-node) model derived from confocal microscopy data [35]. The cell contraction is modeled by applying correlated displacements at specific nodes (representing the focal adhesion sites), e.g., displacing the nodes towards a common center. A force-based stochastic relaxation method is employed to obtain force-balanced network under cell contraction. We find that the majority of the forces are carried by a small number of heterogeneous force chains emitted from the contracting cells. The force chains consist of fiber segments that either possess a high degree of alignment before cell contraction or those that are aligned due to the reorientation induced by the cell contraction. Fluctuations of the forces along different force chains are observed. Importantly, the decay of the forces along the force chains are significantly slower than the decay of radially averaged forces. These results suggest that network structure could support long-range force transmission and thus, long-range mechanical signalling between cells.

The rest of the paper is organized as follows: In Sec.II, we describe our model of biopolymer network and embedded cells. In Sec.III, we provide and validate the force-based relaxation method that minimizes the strain energy of the network to obtain force-balanced network configuration. In Sec.IV, we discuss the properties of stressed biopolymer network due to the contraction of a

single cell. In Sec.V, we present results of the mechanical response of biopolymer network due to the simultaneous contraction of a pair of cells. In Sec.VI, we provide concluding remarks.

## 2. NETWORK AND CELL MODELS

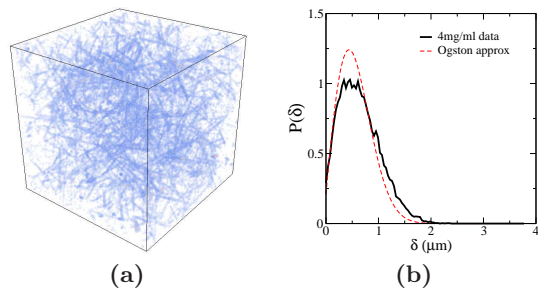


FIG. 1: (Color online). Microstructure of the model biopolymer network studied in this paper (a) and the associated pore-size distribution function  $P(\delta)$  (b). The linear size of simulation box shown in (a) is  $30 \mu\text{m}$ .

The biopolymer network of interest is represented as a graph, i.e., a collection of bonds and nodes [35]. In this model, each bond represents a fiber and each node represents a cross link, see Fig. 1(a) 2. The graph representation is obtained by thresholding and skeletonizing a 3D stack of confocal microscopy images of type I collagen at density of  $4.0 \text{ mg/ml}$ . The average fiber length  $\bar{l}^0 = 1.28 \mu\text{m}$ . A cubic simulation box with a linear size of  $30 \mu\text{m}$  is used, which contains 5,000 nodes and 8,000 bonds. The pore-size distribution function of the network is shown in Fig. 1(b) 2 [55]. Also shown is the Ogston approximation for the pore size distribution, i.e.,

$$P(\delta) = \frac{2\phi_2(\delta + a)}{a^2} e^{-\phi_2(\delta+a)^2/a^2}, \quad (1)$$

where  $\phi_2 = 1 - \phi_1$  is the volume fraction of the fibers and  $a$  is the fiber radius. We note that (1) is derived for networks with very long and stiff fibers, and thus, overestimates the occurrence probability of intermediate sized pores [55].

In order to study the mechanical behavior of the network, we need to specify the properties of individual fibers. In this paper, we assume that the fibers possess short persistent lengths, i.e., the bending modulus of the fibers is significantly smaller than the elongation modulus. In addition, we consider that cell contraction can only generate small forces and thus, the system is in the linear elastic regime [16] and the effects of interstitial fluid, which quickly dissipates the kinetic energy generated due to cell contraction, are not explicitly considered. The mechanically equilibrated network possesses the minimal elastic (strain/stress) energy. The elongation modulus of the fibers is set to be  $EA = 8 \times 10^{-7} N$

[35], where  $E$  is the Young’s modulus of collagen and  $A$  is the cross-section area of the fiber. The elastic energy of a fiber  $\ell_{ij}$  defined by nodes  $i$  and  $j$ ) is a quadric function of fiber elongation, i.e.,

$$\epsilon_{ij} = \frac{EA}{2d_{ij}^0} \cdot (d_{ij} - d_{ij}^0)^2 = k_{ij} \cdot (d_{ij} - d_{ij}^0)^2, \quad (2)$$

where the spring constant of fiber  $k_{ij} = EA/d_{ij}^0$  is inversely proportional to its original length  $d_{ij}^0$ . For computational convenience, the coordinates of the nodes inside the  $30\mu\text{m} \times 30\mu\text{m} \times 30\mu\text{m}$  box are rescaled to fit in a  $1 \times 1 \times 1$  simulation box. In the subsequent calculations, the unit of length is thus chosen to be the length of the simulation box. We note that the results can be easily rescaled to the actual units in order to compare with experimental measurements. The total elastic energy associated with the fiber network is given by

$$E_G = \sum_{\langle i j \rangle} \epsilon_{ij} \quad (3)$$

where the summation is over all pairs of connected nodes (i.e., all fibers  $\ell_{ij}$ ).

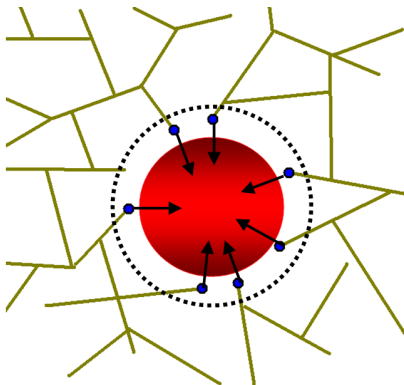


FIG. 2: (Color online). A schematic illustration of our cell contract model. We model an embedded cell as a sphere with radius  $R_c$  (red circle) centered at a prescribed location in the network (dark yellow lines). The nodes of the network within a certain distance  $\delta R$  to the cell surface (i.e.,  $R_c + \delta R$  to the cell center) are considered as “coarse-grained” focal adhesion sites (blue dots). Cell contraction is then modeled by displacing the focal adhesion nodes towards the cell center with a prescribed magnitude.

We model an embedded cell as a spherical region with radius  $R_c$  centered at a prescribed location in the network. Although actual cells generally possess much more complex morphology, such a simple shape is sufficient for our current study, which focuses on heterogeneous force chains generated due to cell contraction. The nodes of the network within a certain distance  $\delta R$  to the cell surface (i.e.,  $R_c + \delta R$  to the cell center) are considered as “coarse-grained” focal adhesion sites, through which the cell is mechanically coupled with the network [56]. Cell

contraction is then modeled by displacing the focal adhesion nodes towards the cell center with a prescribed magnitude. In particular, with the boundary nodes kept fixed (a node is a boundary node if its distance to the box boundary is smaller than 5% of the box length), the set of adhesion nodes are displaced towards to cell center and then kept fixed. This local perturbation leads to a stressed network and the resulting force-balanced configuration is obtained via a force-based stochastic relaxation method (described in detail below): All of the other nodes (free nodes) are allowed to be displaced until the entire network settles down in a new configuration with minimal strain/stress energy minima such that all free nodes are in a force balanced state.

### 3. FORCE-BASED RELAXATION METHOD

Here, we employ a stochastic optimization scheme to find the force-balanced network configuration under the prescribed local perturbations that mimic cell contraction. The standard stochastic optimization procedure consists of a random walk in the configuration space. Specifically, in order to find the minimal energy states, a randomly selected node of the network is given a random small displacement (i.e., a trial move), which leads to stretching/compression of fibers that connected to this node and thus, causes a change of total elastic energy  $E_G$  of the network. If  $E_G$  decreases, the displacement is accepted, otherwise, it is rejected, i.e., the steepest descent method is utilized.

In this scheme, the global energy needs to be recomputed after each trial displacement. Directly recomputing  $E_G$  using Eq. (3) is both time consuming and computationally inefficient due to the large number of nodes (5000) and bonds (8000) in our system, as well as the large number of trial moves (i.e.,  $\sim 5000$  moves for each node). Therefore, a local energy update method [57–59] is employed: before displacing the randomly chosen node, the energy associated with this node, i.e., the “local energy”  $E_L$ , which is defined as the elastic energy of all the bonds (fibers) connected to this specific node, is calculated. Because the displacement of a node only affect the bonds connected to this node, the change of the total energy  $\delta E_G$  is exactly equal to the change this local energy  $\delta E_L$ , i.e.,  $\delta E_G = \delta E_L$ . The acceptance probability of the trial move  $p_{acc}$  is simply given by

$$p_{acc} = \begin{cases} 1, & \delta E_L \leq 0 \\ 0, & \delta E_L > 0. \end{cases} \quad (4)$$

This also enables of the efficient computation of both the global energy and thus, significantly reduces the computational cost, i.e., from 8 CPU hrs to 0.6 CPU hrs on our Dell Precision workstation [with Intel Xeon(R) E5-1603 2.80GHz 4-core CPU and 16 GB Memory].

Furthermore, instead of randomly displacing the nodes, force-based displacements are used. Specifically,

a randomly selected node is displaced along the direction of the net force on this node, with the magnitude of the displacement proportional to the magnitude of the force. For a randomly selected node  $i$ , the net force  $\mathbf{F}^i$  at this node with the components  $F_x^i$ ,  $F_y^i$  and  $F_z^i$  is calculated by summing the  $x$ ,  $y$ ,  $z$  components of all the forces exerted by all the neighbor nodes on this chosen node  $i$ . The magnitude of the force between node  $i$  and its neighbor  $k$  connected by a fiber is computed as

$$f_{ik} = \frac{EA}{d_{ik}^0} \cdot (d_{ik} - d_{ik}^0), \quad (5)$$

where  $E$  is the Young's modulus of the fiber,  $A$  is the fiber cross section area,  $d_{ik}$  and  $d_{ik}^0$  are respectively the fiber lengths after node displacement and original fiber length. Since  $f_{ik}$  is along the direction defined by nodes  $i$  and  $k$ , the  $x$  component of  $f_{ik}$  can be computed by multiplying  $f_{ik}$  by the  $x$  component of the normalized direction vector  $\mathbf{T}^{ik}$  pointing from node  $i$  to  $k$ , i.e.,

$$T_x^{ik} = \frac{(x_k - x_i)}{d_{ik}}, \quad (6)$$

where  $x_i$  and  $x_k$  are respectively the  $x$  coordinates of node  $i$  and  $k$ . The  $x$  component of the net force at node  $i$  is then given by

$$F_x^i = \sum_{\langle k \rangle} f_{ik} \times T_x^{ik}. \quad (7)$$

The components  $F_y^i$  and  $F_z^i$  can be calculated in a similar way, which we do not describe in detail here.

Finally, the node  $i$  is displaced along the direction of  $\mathbf{F}^i$  with a magnitude

$$\delta_i = C \cdot \frac{d_{ik}^0}{EA} \cdot \mathbf{F}^i, \quad (8)$$

where  $C$  is random multiplier between  $[0, 625,000]$ . The upper bound is chosen such that the maximal individual displacement is  $\sim 1/500$  average fiber length, which leads to fast convergence of the optimization. About 5000 trial moves are performed on each node, with an average success rate of 95%. The simulation is terminated when the total energy converge to a stable plateau.

Table I compares the efficiency of different optimization schemes described above. Specifically, the different procedures yield essentially identical final energy, indicating all of them are robust in finding the desired (local) energy minimum. However, the local energy-update scheme accelerates the simulation by 12 times, and the force-based method possesses a success rate that is 20 times higher than the random displacement approach. The differences in the force-based approach and random-displacement approach is also shown in Fig. 3. It can be clearly seen that the force-based scheme significantly improve convergency of the optimization.

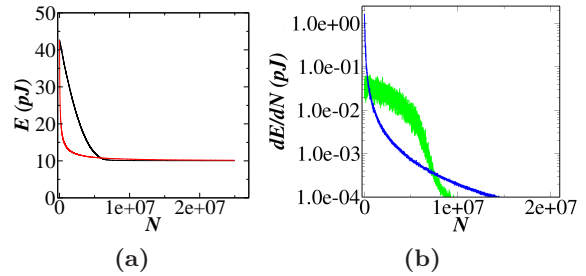


FIG. 3: (Color online). Comparison of different optimization procedures. (a) The total energy (in pJ) as a function of trial move number. The red (or dark gray in print version) curve corresponds to the force-based method and the black curve corresponds to the random displacement method. (b) The rate of change of energy. The blue (or dark gray in print version) curve corresponds to the force-based method and the green (or light gray in print version) curve corresponds to the random displacement method. It can be seen that the force-based scheme significantly improve convergency of the optimization.

#### 4. SINGLE-CELL CONTRACTION RESULTS

In this section, the force-based relaxation method is applied to study the mechanical response of a biopolymer network due to the contraction of a virtual cell embedded in the network. In particular, a spherical cell is placed in the center of the simulation box, i.e. at  $(15, 15, 15)(\mu m)$ , with a radius  $R_c = 4.5 \mu m$  (i.e., a linear size of  $9 \mu m$ ). The contraction ratio  $\Gamma_c$  (defined as the ratio of the cell radius after and before the contraction) is chosen to be 0.3. We consider the ‘‘cell’’ is initially residing inside a stress-free network. Therefore it is easy for the cell to perturb the network via contraction, leading to relatively large  $\Gamma_c$  used here. The force-based relaxation method is then employed to find force-balanced network configuration.

##### 4.1. Heterogeneous distribution of forces on fibers

The distribution of forces on the fibers is shown in Fig. 4. It can be clearly seen that the majority of fibers ( $\sim 5\,000$  out of  $8\,000$  fibers in our system) carries very small forces (i.e., virtually zero). There are only a small number of fibers that carry the majority of the forces  $\sim 10^4$  pN, which leads to a highly heterogeneous distribution of forces in the network.

##### 4.2. Identifying force chains

To understand how the local perturbation due to cell contraction is propagated throughout the system, we investigate the spatial correlations among large-force-bearing fibers and identify well-defined structures formed

	force-based local	random local	force-based global	random global
$t_c$	38 min	40 min	8hr 41min	8hr 59min
$E_G^0$	28.46740	28.46740	28.46740	28.46740
$E_G^f$	6.7716672	6.6983984	6.7727792	6.6982896
$N_t$	25,000,000	25,000,000	25,000,000	25,000,000
$N_s$	23,816,643	1,143,437	23,785,917	1,143,636
$\gamma$	95.3%	4.57%	95.1%	4.57%

TABLE I: Comparison of different stochastic energy minimization schemes to obtained force-balanced biopolymer network configurations.  $t_c$  is the total CPU computational time consumed,  $E_G^0$  is the initial energy (in  $pJ$ ),  $E_G^f$  is the final energy (in  $pJ$ ),  $N_t$  is the total number of MC moves,  $N_s$  is the number of successfully MC moves, and  $\gamma = N_s/N_t$  is the success rate.

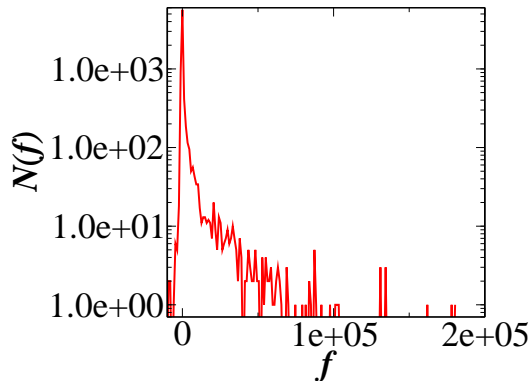
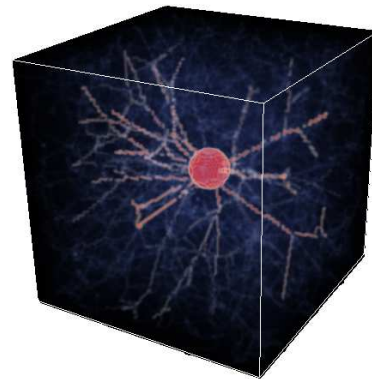


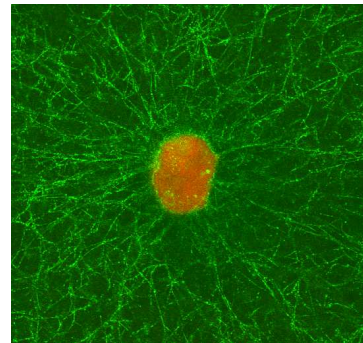
FIG. 4: (Color online). Distribution of forces (in  $pN$ ) on the fibers. The majority of fibers ( $\sim 5000$  out of 8 000 fiber in our system) carries very small forces. There are only a small number of fibers that carry the majority of the forces  $\sim 10^4 pN$ . Such fibers form linear structures, which we refer to as force chains (see Fig. 5).

by these fibers. Specifically, we visualize the entire system in a  $100 \times 100 \times 100$  voxel-based box, with different color code corresponding to different stress states of the fibers. The gradual change of color from blue to red indicates the increase of the forces carried by the fibers. Surprisingly, we find that there are well-defined chain-like structures composed of large-force-bearing fibers (i.e., red fibers) in the network, which are emitting from the contracted cell, i.e., the spherical region centered at  $(15, 15, 15)$  ( $\mu m$ ) and protruding outwards along the radial direction, see Fig. 5(a). We refer to these chain-like structures as “force chains” in the biopolymer network. Figure 5(b) shows the snapshot of a contracting NIH 3T3 cell with an almost spherical morphology in collagen I gel with a concentration of 1.5mg/ml. Similar linear chain-like structures of collagen fibers emitting from the cell can be clearly observed, which validates our simulation.

Starting from the contracted spherical cell, we track the propagation of forces (generated by the cell) along the force chains. In particular, the origin of a force chain is associated with a fiber that is directly connected to the cell, i.e., with one node as the coarsen-grained “focal adhesion” site, points outwardly from the cell and car-



(a)



(b)

FIG. 5: (Color online). Force chains in the biopolymer network due to the contraction of an embedded spherical cell. (a) Simulation result: the fibers carrying large forces are highlighted with red color. It can be clearly seen that there are chain-like structures emitted from the contracted cell, consisting of fibers bearing very large forces ( $\sim 10^4 pN$ ). (b) Experimental validation: A contracting NIH 3T3 cell with an almost spherical morphology in collagen I gel with a concentration of 1.5mg/ml. Similar linear chain-like structures of collagen fibers emitting from the cell can be clearly observed.

ries a force larger than a threshold value (e.g.,  $10^4 pN$ ). The next segment of the force chain is then identify as the fiber that shares a common node of the origin fiber, points outwardly from the cell and carries a force that is

larger than all of the other fibers connected to the shared node. This process is repeated until the force chain extends to the boundary of the box. Although it is not the only way to identify force chains, our procedure identifies force chains with largest linear extent by imposing the condition that the segments of the force chain always point outwardly from the cell. This allows us to investigate the range of fiber-mediated mechanical signaling between cells.

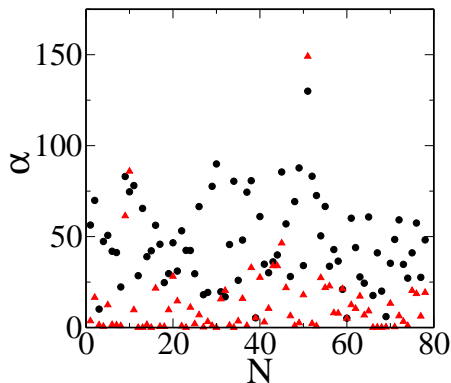


FIG. 6: (Color online). Comparison of the angles  $\alpha$  between two successive fiber segments along the force chains before (black dots) and after (red dots) the cell contraction. This comparison reveals two mechanisms for force-chain formation, i.e., fiber re-orientation and selection of pre-existing chain-like structures in the network, as discussed in the text.

How does such chain-like structures arise in response to the perturbation due to cell contraction? To investigate the mechanism for the formation of such linear structure, we compare the angles  $\alpha$  between two successive fiber segments along the force chains, before and after the cell contraction. Figure 6 shows the comparison. It can be clearly seen that most of the angles  $\alpha$  after cell contraction (shown as red dots) are relatively small (i.e., less than 20 degrees), which is consistent with observed linear chain-like structures. However, a significant fraction of  $\alpha$  ( $\sim 70\%$ ) before contraction (shown as black dots) possesses large values (e.g.,  $> 40$  degrees). This suggests that roughly 70% fibers undergo large re-orientation due to cell contraction in order to support the propagation of forces through the linear force chains. We note this result is consistent with those reported in Ref. [14]. The remaining angles, whose values before the contraction are relatively small, do not significant change after the perturbation. This indicates that certain pre-existing chain-like structures in the non-stressed network can also be selected to carry large forces and contribute to the force chains. The relative contributions of the aforementioned two mechanisms for force-chain formation, i.e., fiber orientation and selection of pre-existing linear structures, generally depends on the network of microstructure.

### 4.3. Force decay along force chains

To quantify how the stress propagates along the force chains, the fiber segments along each force chain have been identified and the magnitude of the forces on the fibers along each force chain are obtained. Figure 7 shows the comparison of the decay of forces along the force chains  $f_C(r)$  and the decay of radially averaged force  $\bar{f}(r)$  as the distance  $r$  from the contracted cell increases. We note that  $\bar{f}(r)$  is computed by averaging the magnitude of forces carried by the fiber segments whose centers are in a concentric thin spherical shell with radius  $r$  and thickness  $\Delta r$ .

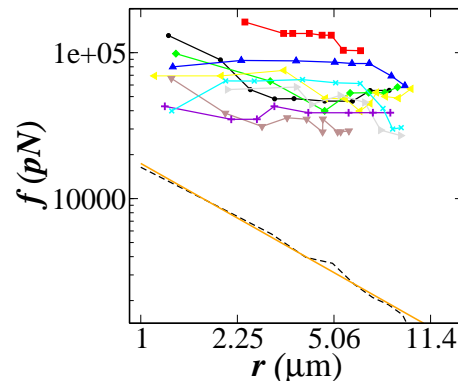


FIG. 7: (Color online). Comparison of the decay of forces  $f_C$  (in  $pN$ ) from the contracting cell along the force chains (solid symbols) and the decay of radially averaged force  $\bar{f}$  (in  $pN$ ) in the biopolymer network (dashed line). It can be clearly seen that the decay of  $f_C$  is much slower than decay of  $\bar{f}$ . This suggests a possible mechanism for long-range force transmission in cellularized biopolymer network.

It can be clearly seen in Fig. 7 that the decay behavior of  $f_C(r)$  is distinctly different than  $\bar{f}(r)$ . In particular,  $f_C(r)$  decays much slower than  $\bar{f}(r)$ , although both are characterized by a power law decay as can be clearly seen in the logarithmic plot. The orange line shows the linear fit of  $\ln \bar{f}$  vs.  $\ln r$ , i.e.,

$$\ln \bar{f}(r) = 9.765 - 1.062 \ln r. \quad (9)$$

The slope 1.062 indicates that the decay of  $\bar{f}(r)$  can be very well described via

$$\bar{f}(r) \sim 1/r, \quad (10)$$

which is consistent with the prediction from linear elastic theory [60]. Due the large fluctuations of the forces along the force chain, the exact decay behavior of  $f_C(r)$  is difficult to extract, but can be approximated via

$$f_C(r) \sim 1/r^\eta, \quad (11)$$

where  $\eta \in (0.3, 0.5)$ . In addition, the magnitude of the forces along the force chain is much higher than the radially averaged forces. This is consistent with our observation from the distribution of forces shown in Fig. 4, i.e.,

the majority of forces are carried by a small number of fibers constituting the force chains, while the remaining fibers carry very small forces (see fig5 & fig7) 5).

## 5. DOUBLE-CELL CONTRACTION RESULTS

To further understand fiber-mediated mechanical coupling between cells, we investigate the force chains formed due to the contraction of two cells that are close to one another. In particular, two cells with  $R_c = 4.5\mu\text{m}$  are placed on the diagonal line of the cubic simulation box, respectively at  $(10.5, 10.5, 10.5)\mu\text{m}$  and  $(19.5, 19.5, 19.5)\mu\text{m}$ . We note that these points are the trisection points of the body diagonal of the “free” part of the simulation box. A contraction ratio of  $\Gamma_c = 0.5$ , instead of 0.3 for the single cell case, is employed. This is because when more than one cells are embedded in the network, the system can be considered in a prestressed state and thus, is more difficult to mechanically perturb than the single cell case. After the perturbation (i.e., simultaneous contraction of both cells), the system is equilibrated using the force-based relaxation method. Specifically, each node is given on average 7,000 trial moves with an average success rate of 97.35%.

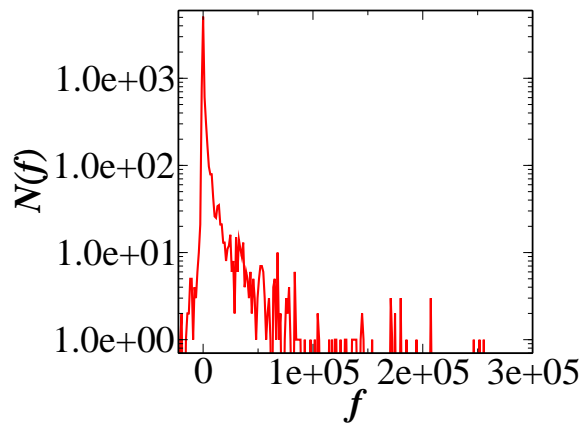
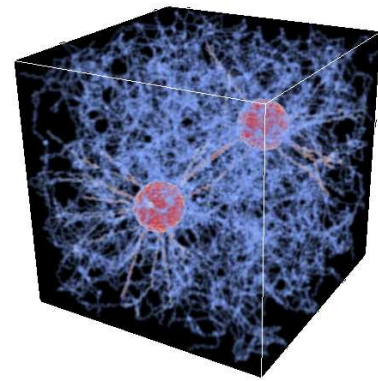
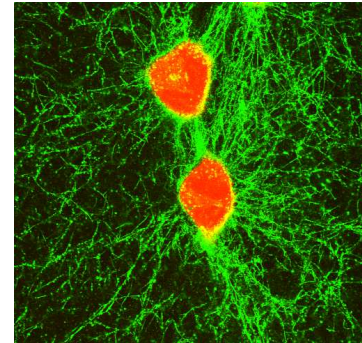


FIG. 8: (Color online). Distribution of the forces (in  $pN$ ) carried by the fibers in the biopolymer network with two contracting cells. It can be seen that the majority of fibers only carry very small forces close to zero. The larger forces are mainly carried by fibers forming force chaining connecting the two contracting cells and emitting outward to the boundary.

Figure 8 shows the distribution of the forces carried by the fibers. As in the single-cell case, the majority of fibers only carry very small forces close to zero. The majority of forces are carried by a small number of fibers which, as shown below, form linear chain-like structures. Figure 9 shows the stressed network due to contraction of the cells. The color code is same as in the single-cell case, i.e., the fibers carrying large forces are highlighted with red color. Two force-chains connecting the two contracting cells can be clearly identified, both consisting fiber elements carrying a forces large than  $10^6$  pN (see Appendix



(a)



(b)

FIG. 9: (Color online). Force chains in the biopolymer network due to the contraction of two embedded cells. (a) Simulation result: The fibers carrying large forces are highlighted with red color. It can be clearly seen that there are chain-like structures connecting the two cells, consisting of fibers bearing very large forces ( $> 10^5$   $pN$ ). (b) Experimental validation: Two contracting NIH 3T3 cells close to one another in collagen I gel with a concentration of 1.5mg/ml. Similar linear chain-like structures of collagen fibers connecting the two cells can be clearly observed.

A). The fibers in the force chains are aligned very well with the body diagonal line, on which the two cells are placed. Figure 9(b) shows the snapshot of two contracting NIH 3T3 cells close to one another in collagen I gel with a concentration of 1.5mg/ml. Similar linear chain-like structures of collagen fibers connecting the two cells can be clearly observed, which validates our simulation.

To understand how such linear-structures form, we compute and compare the angles between individual fiber segments along the force-chains and the body diagonal, before and after cell contraction. Figure 10 shows the comparison. It can be clearly seen that the fiber segments along the two most prominent force chains between the two cells undergo a significant reorientation to align with the body diagonal. We note that in this configuration, the largest forces occur along the body diagonal connecting the 2 cells, which also drive the re-orientation of the fibers. In addition, the fiber segments in the force

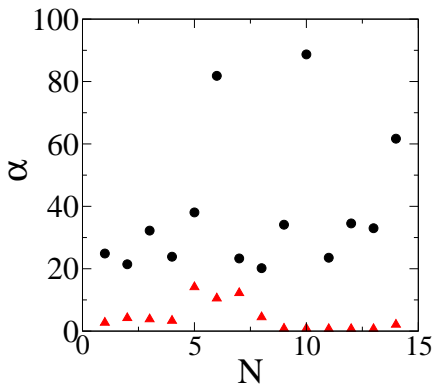


FIG. 10: (Color online). Comparison the angles between individual fiber segment along the force-chains and the body diagonal, before (black dots) and after (red dots) cell contraction. The fiber segments along the force chains undergo a significant reorientation to align with the body diagonal, as discussed in the text. We note that the angles  $\alpha$  shown here are with respect to the body diagonal of the simulation box, rather than the angles between successive fiber segments in the single-cell case.

chain carrying large forces undergo a more significant reorientation (see Appendix A), to get better aligned with the body diagonal in order to resist the larger forces. The “selection” mechanism for force-chain formation is not dominant in the two-cell case. This is because in our current network, the probability of finding a chain of fibers all perfectly aligned with the body diagonal is very small. Finally, we note that since the two-cell configuration does not possess spherical symmetry, we therefore do not characterize the radial decay of the forces, which is not well defined. The magnitude of forces carried by the fiber segments along the force chains are given in Appendix A.

## 6. CONCLUSIONS AND DISCUSSION

We have numerically investigated the mechanical response of a model biopolymer network due to the active contraction of embedded cells. Cell contractions are modeled by applying correlated displacements at specific nodes, representing the focal adhesion sites. A force-based stochastic relaxation method is employed to obtain force-balanced network under cell contraction. We find that the majority of the forces are carried by a small number of heterogeneous force chains emitted from the contracting cells. The force chains consist of fiber segments that either possess a high degree of alignment before cell contraction or are aligned due to the reorientation induced by cell contraction. Large fluctuations of the forces along different force chains are observed [c.f. Fig. 7]. In addition, the decay of the forces along the force chains are significantly slower than the decay of concentric averaged forces in the system. These results

suggest that the fibrous nature of biopolymer network structure can support long-range force transmission and thus, long-range mechanical signaling between cells [61]. One of the advantages of Mechano-signal transduction over Chemical signaling is that it could be upto 40 times faster than the diffusion-based, as is reviewed in [62].

We note that force chains are also apparent in granular materials, which is non-equilibrium state of matter composed of macroscopic particles with strong repulsive interactions [63]. Compared to the typical force chains in granular materials, the force chains we identified in the perturbed network have a much better linearity, i.e., they either aligned radially outwards in the single-cell case or align the body diagonal in the two-cell case. In addition, the forces carried by the fiber segments are stretching forces, while those carried by the individual grains are compressive in nature. The force chains in these two distinct systems also share some similar characteristics. For example, in both systems, the force chains carry the majority of the forces, which are orders of magnitude higher than the average forces carried by a fiber/grain. This implies that the formation of force chains could be a universal mechanism for stress dissipation in disordered systems composed a large number of individual building blocks with interaction rules in between.

Also notably, from Figure 7, we can also see the “duality” of the collagen network system: on one hand, if we are interested in the bulk property of the system, it’s totally fine to treat the collagen network as homogeneous in the same way as all the other continuum materials, which is evident from the perfect  $1/r$  overall decay of the stress field, on the other hand, if we are more intrigued by the underlying events happening at even smaller scales, the fibrous nature of collagen system can not neglect.

Finally, we note that our biopolymer network model only considers fiber elongation and does not explicitly take into account the effect of bending. This assumption works perfectly fine for fibers with short persistent lengths, but is not true for fibers with long persistent lengths. In future work, the effects of fiber bending will be explicitly investigated. In addition, the effects of fiber alignment in the original non-stressed network will also be studied. It is expected that in a highly-orientated fiber network, the “selection mechanism” will dominant for force-chain formations, and thus, significantly biases the force propagation as well as the cell migration inside.

## Acknowledgments

L. L. and Y. J. thank Arizona State University for the generous start-up funds.

### Appendix A: Forces on force chain elements in double-cell configuration

TABLE II: Realignment of the fibers (i.e., change of the angle  $\alpha$  (degree) between two successive fiber segments before and after contraction) in the force chain between the 2 cells and the forces (pN) carried by the fiber segments.

Element	$\alpha$ Before	$\alpha$ After	Force
Force Chain 1			
0	24.87	2.71	174,334.2
1	21.43	4.21	182,937.9
2	32.22	3.83	182,290.5
3	23.85	3.34	181,654.4
4	38.05	14.12	164,516.6
5	81.81	10.51	152,255.8
6	23.30	12.23	169,661.7
Force Chain 2			
0	20.17	4.49	315,013.8
1	34.11	0.81	219,117.7
2	88.69	0.81	219,118.4
3	23.52	0.71	224,975.0
4	34.51	0.72	224,988.8
5	32.98	0.72	224,989.5
6	61.68	2.10	308,953.9

- 
- [1] H. Lodish, A. Berk, S. L. Zipursky, P. Matsudaira, D. Baltimore, and J. Darnell, *Molecular Cell Biology*, 4th Edition, Chapter 22 (W. H. Freeman, 2000).
- [2] A. Ridley et al., *Science* **302**, 1704 (2003).
- [3] J. D. Humphrey, E. R. Dufresne, and M. A. Schwartz, *Nat. Rev. Mol. Cell Biol.* **15**, 802 (2014).
- [4] C. Bonnans, J. Chou, and Z. Werb, *Nat. Rev. Mol. Cell Biol.* **15**, 786 (2014).
- [5] R. J. Pelham, Jr., and Y. Wang, *Proc. Natl. Acad. Sci. USA* **94**, 13661 (1997).
- [6] T. Yeung et al., *Cell Motility and the Cytoskeleton* **60**, 24 (2005).
- [7] A. J. Engler, S. Sen, H. L. Sweeney, and D. E. Discher, *Cell* **126**, 677 (2006).
- [8] K. R. Levental, H. Yu, L. Kass, J. N. Lakins, M. Egeblad, J. T. Erler, S. F. T. Fong, K. Csiszar, A. Giaccia, W. Weninger, et al., *Cell* **139**, 891 (2009).
- [9] R. W. Tilghman, C. R. Cowan, J. D. Mih, Y. Koryakina, D. Gioeli, J. K. Slack-Davis, B. R. Blackman, D. J. Tschumperlin, and J. T. Parsons, *PLoS ONE* **5**, e12905 (2010).
- [10] E. Hadjipanyi, V. Mudera, and R. A. Brown, *Cell Motil. Cytoskeleton* **66**, 121 (2009).
- [11] S. Guido and R. T. Tranquillo, *J. Cell Sci.* **105**, 317 (1993).
- [12] P. P. Provenzano, D. R. Inman, K. W. Eliceiri, S. M. Trier, and P. J. Keely, *Biophys. J.* **95**, 5374 (2008).
- [13] T. R. Cox and J. T. Erler, *Dis. Model Mech.* **4**, 165 (2011).
- [14] H. Wang, A. S. Abhilash, C. S. Chen, R. G. Wells, and V. B. Shenoy, *Biophys. J.* **107**, 2592 (2014).
- [15] R. K. Sawhney and J. Howard, *J. Cell Biol.* **157**, 1083 (2002).
- [16] X. Ma, M. E. Schickel, M. D. Stevenson, A. L. Sarang-Sieminski, K. J. Gooch, S. N. Ghadiali, and R. T. Hart, *Biophys. J.* **104**, 1410 (2013).
- [17] Q. Shi, R. P. Ghosh, H. Engelke, C. H. Rycroft, L. Cassereau, J. A. Sethian, V. M. Seaver, and J. T. Liphardt, *Proc. Nat. Acad. Sci.* **111**, 658 (2014).
- [18] T. Lecuit, P. Lenne, and E. Munro, *Annu. Rev. Cell Dev. Biol.* **27**, 157 (2011).
- [19] R. Fernandez-Gonzalez, M. S. Simoes, J. C. Röper, S. Eaton, and J. A. Zallen, *Dev. Cell* **17**, 736 (2009).
- [20] G. Totsukawa, Y. Wu, Y. Sasaki, D. J. Hartshorne, Y. Yamakita, S. Yamashiro, and F. Matsumura, *J. Cell Biol.* **164**, 427 (2004).
- [21] K. Jakab, A. Neagu, V. Mironov, R. R. Markwald, and G. Forgacs, *Proc. Natl. Acad. Sci. USA* **101**, 2864 (2004).
- [22] P. Friedl and D. Gilmour, *Nat. Rev. Mol. Cell Biol.* **10**, 445 (2009).
- [23] M. A. Wozniak and C. S. Chen, *Nat. Rev. Mol. Cell Biol.* **10**, 34 (2009).
- [24] D. E. Jaalouk and J. Lammerding, *Nat. Rev. Mol. Cell Biol.* **10**, 63 (2009).

- [25] M. E. Lukashev and Z. Werb, *Trend. Cell Biol.* **8**, 437 (1998).
- [26] S. R. Gujarathi, C. L. Farrow, C. Glosser, L. Granlund, and P. M. Duxbury, *Phys. Rev. E* **89**, 053311 (2014).
- [27] F. J. O'Brien, B. A. Harley, M. A. Waller, I. V. Yannas, L. J. Gibson, and P. J. Prendergast, *Tech. Health Care* **15**, 3 (2007).
- [28] Y. L. Yang, S. Motte, and L. J. Kaufman, *Biomaterials* **31**, 5678 (2010).
- [29] A. G. Ogston, *Trans. Faraday Soc.* **54**, 1754 (1958).
- [30] A. R. Takahashi, R. Kita, T. Shinozaki, K. Kubota, and M. Kaibara, *Colloid Polym. Sci.* **281**, 832 (2003).
- [31] W. Mickel and et al, *Biophys. J.* **95**, 6072 (2008).
- [32] Y. Jiao and S. Torquato, *Phys. Biol.* **9**, 036009 (2012).
- [33] A. O. Brightman, B. P. Rajwa, J. E. Sturgis, M. E. McCallister, J. P. Robinson, and S. L. Voytik-Harbin, *Biopolymers* **54**, 222 (2000).
- [34] J. Zhu and L. J. Kaufman, *Biophys. J.* **106**, 1822 (2014).
- [35] S. B. Lindström, D. A. Vader, A. Kulachenko, and D. A. Weitz, *Phys. Rev. E* **82**, 051905 (2010).
- [36] C. A. R. Jones, L. Liang, D. Lin, Y. Jiao, and B. Sun, *Soft Matter* **10**, 8855 (2014), ISSN 1744-6848.
- [37] R. K. Jain, *Cancer Res.* **47**, 3039 (1987).
- [38] A. G. Ogston, B. N. Preston, and J. D. Wells, *Proc. R. Soc. London A* **333**, 297 (1973).
- [39] L. Johansson, U. Skantzle, and J. E. Löfroth, *Macromolecules* **24**, 6019 (1991).
- [40] L. Johansson and J. E. Löfroth, *Colloid Interface Sci.* **142**, 116 (1991).
- [41] L. Johansson, C. Elvingson, and J. E. Löfroth, *Macromolecules* **24**, 6024 (1991).
- [42] L. Johansson and J. E. Löfroth, *J. Phys. Chem.* **98**, 7471 (1993).
- [43] H. A. Leddy, M. A. Haider, and F. Guilak, *Biophys. J.* **91**, 311 (2006).
- [44] A. E. et al., *Biopolymers* **89**, 135 (2008).
- [45] T. Stylianopoulos, B. Diop-Frimpong, L. L. Munn, and R. K. Jain, *Biophys. J.* **99**, 3119 (2010).
- [46] A. P. Chatterjee, *J. Phys.: Condens. Matter* **23**, 375103 (2011).
- [47] Y. Yang, L. M. Leone, and L. J. Kaufman, *Biophys. J.* **97**, 2051 (2009).
- [48] C. B. Raub, A. J. Putnama, B. J. Tromberg, and S. C. George, *Acta Biomaterialia* **6**, 4657 (2010).
- [49] C. P. Broedersz, X. Mao, T. C. Lubensky, and F. C. MacKintosh, *Nat. Phys.* **7**, 983 (2011).
- [50] J. Feng, X. Mao, and L. M. Sander, *arXiv:1402.2998* (2014).
- [51] H. Jiang, L. Jiang, J. D. Posner, and B. D. Vogt, *Comput. Mech.* **42**, 607 (2006).
- [52] J. Zhang, X. Zhao, Z. Suo, and H. Jiang, *J. Appl. Phys.* **105**, 093522 (2009).
- [53] C. P. Broedersz, X. Mao, T. C. Lubensky, and F. C. MacKintosh, *Nat. Phys.* **7**, 983 (2011).
- [54] M. Tozluoğlu, A. L. Tournier, R. P. Jenkins, S. Hooper, P. Bates, and E. Sahai, *Nat. Cell Biol.* **15** (2013).
- [55] Y. Jiao and S. Torquato, *AIP Advances* **2**, 011003 (2012).
- [56] S. V. Plotnikov and C. M. Waterman, *Current opinion in cell biology* **25**, 619 (2013).
- [57] Y. Jiao, F. H. Stillinger, and S. Torquato, *Phys. Rev. E* **76**, 031110 (2007).
- [58] Y. Jiao, F. H. Stillinger, and S. Torquato, *Phys. Rev. E* **77**, 031135 (2007).
- [59] Y. Jiao, F. H. Stillinger, and S. Torquato, *Proc. Natl. Acad. Sci. USA* **106**, 17634 (2009).
- [60] S. Torquato, *Random Heterogeneous Materials: Microstructure and Macroscopic Properties*. New York: Springer-Verlag (2002).
- [61] N. Wang, J. D. Tytell, and D. E. Ingber, *Nature reviews Molecular cell biology* **10**, 75 (2009).
- [62] S. Na, O. Collin, F. Chowdhury, B. Tay, M.X. Ouyang, Y.X. Wang, and N. Wang, *Proc. Natl. Acad. Sci. USA.* **105**, 6626 (2008).
- [63] J. Peters, M. Muthuswamy, J. Wibowo, and A. Tordesillas, *Physical review E* **72**, 041307 (2005).